

FACTORIZED BINARY SEARCH: CHANGE POINT DETECTION IN THE NETWORK STRUCTURE OF MULTIVARIATE HIGH-DIMENSIONAL TIME SERIES

BY MARTIN ONDRUS^{1,2,*}, EMILY OLDS^{1,†} AND IVOR CRIBBEN^{1,2,‡}

¹Alberta School of Business, Canada

²Neuroscience and Mental Health Institute, University of Alberta, Canada
*mondrus@ualberta.ca; †eolds@ualberta; ‡cribben@ualberta.ca

Functional magnetic resonance imaging (fMRI) time series data presents a unique opportunity to understand temporal brain connectivity, and models that uncover the complex dynamic workings of this organ are of keen interest in neuroscience. Change point models can capture and reflect the dynamic nature of brain connectivity, however methods that translate well into a high-dimensional context (where $p \gg n$) are scarce. To this end, we introduce *factorized binary search* (FaBiSearch), a novel change point detection method in the network structure of multivariate high-dimensional time series. FaBiSearch uses non-negative matrix factorization, an unsupervised dimension reduction technique, and a new binary search algorithm to identify multiple change points. In addition, we propose a new method for network estimation for data between change points. We show that FaBiSearch outperforms another state-of-the-art method on simulated data sets and we apply FaBiSearch to a resting-state and to a task-based fMRI data set. In particular, for the task-based data set, we explore network dynamics during the reading of Chapter 9 in *Harry Potter and the Sorcerer's Stone* and find that change points across subjects coincide with key plot twists. Further, we find that the density of networks was positively related to the frequency of speech between characters in the story. Finally, we make all the methods discussed available in the R package **fabisearch** on CRAN.

1. Introduction. Functional magnetic resonance imaging (fMRI) is widely used as an indirect method of measuring brain activity using the blood-oxygen-level-dependent (BOLD) signal (Ogawa et al., 1990). With increases in neuronal activity, glucose and oxygen must be delivered to the neurons from the blood stream causing an increase in oxyhemoglobin to localize nearby. This subsequently increases the ratio of oxyhemoglobin to deoxyhemoglobin, and provides the basis of measurement of the BOLD signal in fMRI. Typically, multiple slices of the subject's brain are scanned and then divided into small (a few millimeters in dimension) cubes called voxels. By taking multiple scans of each slice sequentially over time, a time series of voxel activity can be created.

With the advent of ever increasing computational capacity, and general interest in scalable, data-driven techniques for characterizing neurological phenomena, fMRI data presents a unique opportunity. By studying the relationships among voxels (or a cluster of voxels often referred to as regions of interest, or ROIs) in a brain, we can better characterize brain connectivity leading to a greater understanding of the brain and extensive clinical implications (Bullmore and Sporns, 2009; Sporns, 2011). Functional connectivity (FC) seeks to define the relationships (Biswal et al., 1995) by means of correlation, covariance, and precision matrices amongst other techniques (see Cribben and Fiecas (2016) for a review). Network theory remains at the core of most FC based estimation methods, and for good reason; it intuitively represents the brain as a network with ROIs as nodes and temporal dependence as edges.

Keywords and phrases: time series, high-dimensional, change point detection, NMF, fMRI, network analysis.

Typically however, these methods assume that the FC between the ROIs remains constant throughout the duration of the experiment. While this reduces computational time and complexity, it fails to capture the evolving and dynamic nature of the brain. Evidence of a changing, non-stationary FC over the experiment has been demonstrated in both resting-state data (Delamillieure et al., 2010; Doucet et al., 2012) and task-based experiments (Fox et al., 2005; Debener et al., 2006; Eichele et al., 2008; Cribben, 2012).

Numerous statistical methods have emerged to capture and express the dynamic nature of FC. First, moving window approaches adapt covariance, correlation, or precision matrix methods into a time-varying context. These approaches define sequential blocks of time points and estimate FC within each block. By determining FC across blocks from the beginning to the end of the time course, time-varying FC can be estimated (see Hutchison et al. (2013) for a review). Although the moving-window approach is a computationally practical way of determining FC, it has limitations (Hutchison et al., 2013). For one, the resulting FC patterns are heavily influenced by the choice of block size, which can result in vastly different FC patterns. Additionally, this technique gives no weight to time points outside of those included in the window.

Instead of a moving window, change point methods have also been applied to this problem. Here, we are attempting to find the optimal windows for stationary structures. There exists an extensive literature and a long history on change points beginning with Page (1963). The most widely discussed problems have been concerned with finding change points in univariate time series and more recently, to detecting multiple change points in multivariate time series. For example, Aue et al. (2009) introduced a method to detect changes in the covariance matrix of a multivariate time series, Dette and Wied (2016) proposed a test where the dimension of the data is fixed while recently Kao et al. (2018) considered the case where the dimension of the data increases with the sample size (they also investigated change point analysis based on Principal Component Analysis). Sundararajan and Pourahmadi (2018) proposed a new method for detecting multiple change points in the covariance structure of a multivariate piecewise-stationary process. Using a combination of principal components analysis (PCA) and wavelets to transform the time series, Cho and Fryzlewicz (2015) segmented the multivariate time series into partitions based on the second-order structure.

There have also been many new methods developed for neuroimaging data. Cribben et al. (2012) first introduced a change method for estimating dynamic functional connectivity by considering change points in precision matrices (undirected graphs) using binary segmentation and the bayesian information criterion metric. Accordingly, Cribben, Wager and Lindquist (2013); Schröder and Ombao (2015); Kirch, Muhsal and Ombao (2015); Gibberd and Nelson (2014); Avanesov et al. (2018); Dai, Zhang and Srivastava (2019); Anastasiou, Cribben and Fryzlewicz (2020) then proposed further methods for estimating FC change points. Mosqueiro et al. (2016); Koepcke, Ashida and Kretzberg (2016); Xiao et al. (2019) also considered change points in spike trains. While these methods are effective, they all are limited in the number of time series that can be considered. Subsequently, there has been a drive to extend techniques to high-dimensional spaces, specifically the case $p \gg T$, where p is the number time series variables and T is the total length of the time series. To this end, Cribben and Yu (2017) introduced the network change point detection method, which uses both change point and community detection techniques to estimate change points by examining the time evolving community network structure of multivariate time series. In addition, Ofori-Boateng, Gel and Cribben (2020) introduced a new method that firstly presents each network snapshot of fMRI data as a linear object and finds its respective univariate characterization via local and global network topological summaries and then adopts a change point detection method for (weakly) dependent time series based on efficient scores.

In this paper, we introduce a new method, called *factorized binary search* (FaBiSearch), to detect multiple change points in the network (or clustering) structure of multivariate high-dimensional time series. FaBiSearch has the following unique and important attributes. First, FaBiSearch is, to the best of our knowledge, the first statistical method to use non-negative matrix factorization (NMF) for finding change points in the network (or clustering structure) in multivariate high-dimensional time series. NMF is an unsupervised method of dimension reduction and clustering commonly used in text analysis. Second, FaBiSearch is suitable for detection of multiple change points. Third, FaBiSearch is scalable ($p \gg T$) in that it is unconstrained to the dimensionality of the problem space and is therefore ideal for determining large, changing network structures, such as those in the brain. For the simulated data sets we consider in this work, we find that FaBiSearch has a superior performance to previous state-of-the-art methods. In addition, for simulations where the subject alternates between two states (such as task-based fMRI data), FaBiSearch performs very well and clearly outperforms the other methods. Fourth, FaBiSearch uses a new binary search algorithm to identify multiple change points. Fifth, the NMF element of FaBiSearch allows us to define a new method for the estimation of networks for data between change points. Sixth, FaBiSearch allows for the exploration of high-dimensional network dynamics during a test-retest resting-state fMRI experiment, and a task-based fMRI experiment (the reading of Chapter 9 in *Harry Potter and the Sorcerer's Stone*) for the detection of change points across subjects that coincide with key plot twists. Further, we can use it to find that the density of networks was positively related to the frequency of speech between characters in the story. Seventh, while motivated by fMRI data, FaBiSearch is also applicable to electroencephalography (EEG), magnetoencephalography (MEG) and electrocorticography (ECoG) data, and other high-dimensional time series applications where the network, community or clustering structure is changing over time. Finally, the R package **fabisearch** implementing the methods is available from CRAN ([Ondrus and Cribben, 2021](#)).

The setup of this paper is as follows. In Section 2, we describe our novel method, FaBiSearch, and the new method for estimating networks between pairs of change points. In Sections 3, we describe the simulated and fMRI data sets and we outline the results in Section 4. We have a discussion in Section 5 before concluding in Section 6.

2. Methods. In this section, we first describe non-negative matrix factorization (NMF). Next, we introduce our Factorized Binary Search (FaBiSearch) method.

2.1. Non-negative matrix factorization. NMF is a matrix factorization technique which constrains the input matrix and subsequent factors to non-negative values ([Lee and Seung, 2001](#)). It is commonly used as an unsupervised dimension reduction method and allows for high-dimensional data sets to be projected into simpler and ultimately more workable dimensions. NMF has the following setup: consider an $n \times p$ matrix, \mathbf{X} , where n is the number of independent samples and p is the number of features. NMF attempts to approximate the original matrix \mathbf{X} , as the dot product of a coefficient matrix, \mathbf{W} , and a basis matrix, \mathbf{H} (Figure 1). The dimensionality of factors \mathbf{W} and \mathbf{H} is controlled by the factorization rank, r , where $r \ll \min(n, p)$. The rank is ideally chosen to be large enough such that $\mathbf{W} \cdot \mathbf{H}$ retains key structural elements of \mathbf{X} while also low enough such that the addition of noise has a minimal effect; choosing the rank is key for managing the bias-variance tradeoff. The interpretation of rank is dependent on context, however, due to the clustering property of NMF ([Li et al., 2014](#); [Li and Ma, 2004](#)), we can intuitively think of it as the number of unique clusters in \mathbf{X} .

Finding the loss between \mathbf{X} and factorization $\mathbf{W} \cdot \mathbf{H}$ is an important step for comparing the quality of NMF models. We consider two loss measures that were proposed by [Lee](#)

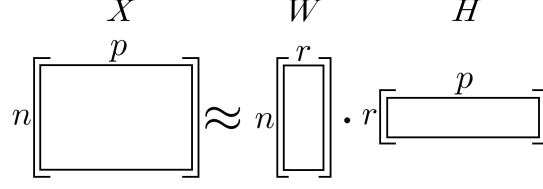


FIG 1. The conceptualization of non-negative matrix factorization (NMF). The $n \times p$ input matrix \mathbf{X} is approximated by the dot product of low dimensional factors \mathbf{W} ($n \times r$ matrix) and \mathbf{H} ($r \times p$ matrix), where $r \ll \min(n, p)$.

and Seung (2001). The first is based on the Euclidian distance between input matrix \mathbf{X} and factorization $\mathbf{W} \cdot \mathbf{H}$,

$$(1) \quad \|\mathbf{X} - \mathbf{W} \cdot \mathbf{H}\|^2 = \sum_{ij} (\mathbf{X}_{ij} - \mathbf{W}_{ij} \cdot \mathbf{H}_{ij})^2,$$

for each ij^{th} entry. The second loss is based on Kullback-Leibler divergence,

$$(2) \quad D(\mathbf{X} \parallel \mathbf{W} \cdot \mathbf{H}) = \sum_{ij} (\mathbf{X}_{ij} \log \frac{\mathbf{X}_{ij}}{\mathbf{W}_{ij} \cdot \mathbf{H}_{ij}} - \mathbf{X}_{ij} + \mathbf{W}_{ij} \cdot \mathbf{H}_{ij}),$$

where the asymmetric divergence between the input matrix \mathbf{X} and the NMF factorization $\mathbf{W} \cdot \mathbf{H}$ is calculated for each ij^{th} entry. In addition to these loss metrics, Lee and Seung (2001) also describe algorithms utilizing multiplicative updates to find factors \mathbf{W} and \mathbf{H} given an input matrix \mathbf{X} . These iterative methods seek to minimize these loss functions.

2.2. NMF change point detection. We adjust the definition of NMF for use in a time series context, where the input multivariate high-dimensional time series $\mathbf{Y} \in \mathbb{R}_{\geq 0}^{T \times p}$ is approximated by the dot product of \mathbf{W} and \mathbf{H} with $r \ll \min(n, T)$:

$$\mathbf{Y}_{T \times p} \approx \mathbf{W}_{T \times r} \cdot \mathbf{H}_{r \times p}.$$

Our new method, FaBiSearch, detects change points in the network structure of a multivariate high-dimension time series with NMF being a core constituent of FaBiSearch. To evaluate how well $\mathbf{W} \cdot \mathbf{H}$ reconstructs \mathbf{Y} , we use the loss metrics proposed by Lee and Seung, namely the Euclidian distance (1) or Kulback-Leibler divergence (2). We expect our NMF reconstruction of the input matrix, \mathbf{Y} , to have a comparatively lower loss when the input shows a clear and consistent clustering structure and/or relationship amongst time series. For an input matrix which contains a change point, we expect NMF to attempt to fit to the dominant temporal structure and to suffer a subsequent higher loss for time points where this structure is different. This leads to a higher observed overall loss for that matrix, as NMF is unable to incorporate multiple, different, clustering structures across all time points. To this end, FaBiSearch is interested in testing the following hypothesis:

$$\begin{aligned} H_0 : & \text{There is no change point in the network structure of } \{\mathbf{Y}_t\}_{t=1}^T \\ H_a : & \text{At an unknown time } t \in \{1, \dots, T\} \text{ a change point occurs in } \{\mathbf{Y}_t\}_{t=1}^T \end{aligned}$$

2.3. Initialization and the factorization rank parameter. As the estimation of \mathbf{W} and \mathbf{H} in FaBiSearch is iterative, it is sensitive to the initial values of these matrices. Hence, to achieve a satisfactory approximation the factorization must be carried out for multiple runs using different initial values for \mathbf{W} and \mathbf{H} . In FaBiSearch, we simply record the best

initialization with the lowest loss. We define the number of runs as n_{run} . Its value attempts to balance accuracy (higher n_{run}) and computational time (lower n_{run}).

As mentioned previously, the factorization rank is a key parameter in NMF. In FaBiSearch, it can be specified beforehand, if known. In many cases, however, it is unknown, hence we also provide a method for finding the optimal rank, which has been adapted from Frigyesi and Höglund (2008). It proceeds as follows: we find the global optimal rank, r_{opt} , by comparing the change in loss in response to increasing rank for the original \mathbf{Y} to a permuted version, \mathbf{Y}^* . For example, using the Euclidean distance loss (1), $\|\mathbf{Y} - \mathbf{W} \cdot \mathbf{H}\|^2$ is computed for different choices of rank and compared to the loss of $\|\mathbf{Y}^* - \mathbf{W}^* \cdot \mathbf{H}^*\|^2$, where \mathbf{Y}^* denotes the expression matrix \mathbf{Y} with the rows (time series) permuted for every column (sample). The slope in a plot of the loss versus rank r is a measure of how much information is lost as the rank decreases. If the slope of the loss of \mathbf{Y} is larger than that of \mathbf{Y}^* this indicates information present in the original data set. The change in loss is compared iteratively and the optimal rank, r_{opt} , is the first rank where the change in loss for \mathbf{Y} is less than \mathbf{Y}^* .

2.4. Segmentation using modified binary search. As FaBiSearch requires a block of data to compute the factorization we define the parameter, δ , as the minimum distance between candidate change points. It is a user defined variable in FaBiSearch and should be small enough such that change points are not missed but should be large enough that statistical power is preserved. Thus, we define the boundary of candidate change points, t_{start} and t_{end} , as δ time units from the beginning, t_{min} , and the end, t_{max} , of the time series.

The most commonly used change point segmentation method is binary segmentation. Here, all possible indices from t_{start} to t_{end} are sequentially evaluated to find the time point, t , where some criterion is maximized or minimized (Douglas and Peucker, 1973; Ramer, 1972; Duda and Hart, 1974). The method can be recursively applied to find multiple change points. For multivariate high-dimensional time series, applying NMF to each candidate change point with a large number of runs ($n_{run} \gg 1$) is computationally very intense. As such, we propose a new efficient segmentation method for finding the global maxima/minima of our chosen criterion (loss) for detecting candidate change points. Binary search is a greedy algorithm typically to find the position of values in a sorted array. By iteratively halving the search space, binary search improves upon a sequential search by reducing the worst case search size from $O(T)$ to $O(\log T)$, where T is the number of time points to be evaluated (that is, from t_{start} to t_{end}). We deploy binary search in FaBiSearch method with the core concept being that for two multivariate time series where one has a change point, all else being equal, the time series with the change point will have a higher loss, l (1 and 2) when NMF is fit.

The setup of the binary search is as follows. Suppose $\hat{Q} = (\hat{q}_1, \hat{q}_2, \dots, \hat{q}_{\hat{M}})$ represent the \hat{M} candidate change points. The objective of our adapted binary search is to find an overlap between two unique clustering structures (Figure 2). By overlapping the left and right block and centering over the mid point of the time points we are guaranteed that one of the blocks includes a candidate change point \hat{q}_1 , if one exists. Adding δ worth of “padding” to the left and right side also ensures the block always contains δ time points; the left and right blocks are always large enough to make meaningful comparisons (Algorithm 1). After the first candidate change point is found, we define two child matrices, $\{\mathbf{Y}_t\}_1^{\hat{q}_1}$ and $\{\mathbf{Y}_t\}_{\hat{q}_1+1}^T$. The modified binary search algorithm is applied to each of these child matrices recursively.

2.5. Refitting segments. Once FaBiSearch has been exhausted, and we have detected (possibly) multiple candidate change points, we carry out a refitting procedure. The first step is to divide \mathbf{Y} into segments defined by the boundaries of the time series and the candidate change points, \hat{Q} . For the general case, consider the boundary set, $b \leftarrow \{1, \hat{Q}, T\}$, where

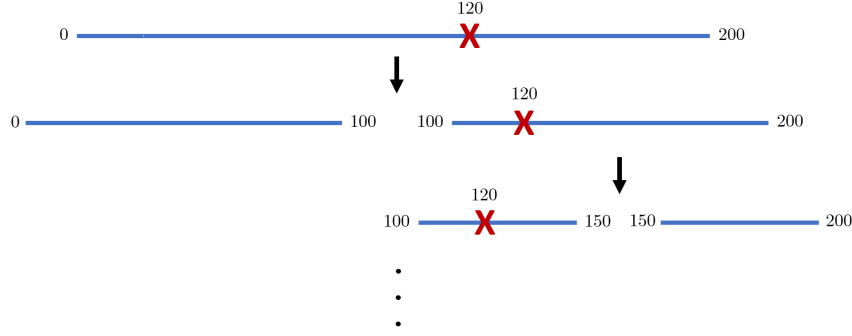


FIG 2. A graphic of the first two iterations of the modified binary search procedure for FaBiSearch. The multivariate time series ($T = 200$) denoted by the blue line, is progressively divided to find the true change point ($t^* = 120$) denoted by the red cross.

the candidate change points \hat{Q} have been arranged in ascending order. Next, consider the corresponding left and right boundaries for candidate change point, \hat{q}_i ,

$$b_i^L \leftarrow b(b^{-1}(\hat{q}_i) - 1); b_i^R \leftarrow b(b^{-1}(\hat{q}_i) + 1).$$

We then define the data segment for \hat{q}_i as $\mathbf{Z}_i \leftarrow \{\mathbf{Y}_t\}_{b_i^L}^{b_i^R}$ and the corresponding sub-segments \mathbf{Z}_i^L and \mathbf{Z}_i^R which represent the data before and after the candidate change point \hat{q}_i as

$$\mathbf{Z}_i^L \leftarrow \{\mathbf{Y}_t\}_{b_i^L}^{\hat{q}_i}; \mathbf{Z}_i^R \leftarrow \{\mathbf{Y}_t\}_{\hat{q}_i+1}^{b_i^R}.$$

We re-estimate NMF on data sub-segments \mathbf{Z}_i^L and \mathbf{Z}_i^R and sum the loss (1 or 2). In particular, we calculate the loss

$$l_i = nm f(\mathbf{Z}_i^L) + nm f(\mathbf{Z}_i^R).$$

Then by combining the calculations over n_{reps} a distribution, $l_i = \{l_{i,1}, \dots, l_{i,n_{reps}}\}$, is obtained. To determine whether a candidate change point remains, we compare the distribution generated by the refitting step to a reference distribution, which is generated by first taking the partition associated with the candidate change point, then permuting this segment across time points to disrupt the temporal organization of the clustering structure. For this permuted segment, \mathbf{Z}_i^* the change point we calculate the loss

$$l_i^* = nm f(\mathbf{Z}_i^{*,L}) + nm f(\mathbf{Z}_i^{*,R}).$$

Then by combining the calculations over n_{reps} a permutation distribution of losses, $l_i^* = \{l_{i,1}^*, \dots, l_{i,n_{reps}}^*\}$, is obtained.

2.6. Statistical inference. To determine change points, we use a one-sided, two sample t -test assuming unequal variances between the two distributions. Recall that we expect time series that include a change point to have a higher loss when fitting NMF. If the clustering structure is consistent throughout the data segment, we expect the permutation of the data to not significantly affect the summed losses over multiple runs. However, if the clustering structures before and after the change point are unique, then the summed losses for the original data segment \mathbf{Z}_i should be lower than the same data segment permuted over time points \mathbf{Z}_i^* . Thus, our hypothesis is constructed as such

$$\begin{aligned} H_0 &: \mu(l_i) \geq \mu(l_i^*) \\ H_a &: \mu(l_i) < \mu(l_i^*), \end{aligned}$$

Algorithm 1: A binary search adapted for change point detection. This method is recursively applied to find multiple change points. For the first iteration of the algorithm, t_{min} and t_{max} are time points 1 and T of \mathbf{Y} , respectively.

Inputs: $\mathbf{Y}, t_{min}, t_{max}, \delta, n_{run}, r$
Output: \hat{q}

```

 $t_{start} \leftarrow t_{min} + \delta; t_{end} \leftarrow t_{max} - \delta$ 
 $x \leftarrow \{x \in \mathbb{N} | t_{start} \leq x \leq t_{end}\}$ 
while  $|x| > 1$  do
     $t_{size} \leftarrow |x|/2$ 
    if  $t_{size} \in \mathbb{N}$  then
         $\mathbf{V}^L \leftarrow \mathbf{Y} \in (\min(x) - \delta) : x_{[t_{size}]}$ 
         $\mathbf{V}^R \leftarrow \mathbf{Y} \in x_{[t_{size}]} : (\max(x) + \delta - 1)$ 
    else if  $t_{size} \notin \mathbb{N}$  then
         $t_{size} \leftarrow \lceil t_{size} \rceil$ 
         $\mathbf{V}^L \leftarrow \mathbf{Y} \in (\min(x) - \delta) : x_{[t_{size}]}$ 
         $\mathbf{V}^R \leftarrow \mathbf{Y} \in x_{[t_{size}]} : (\max(x) + \delta)$ 
     $l^L \leftarrow nmf(\mathbf{V}^L); l^R \leftarrow nmf(\mathbf{V}^R)$ 
     $x \leftarrow x$  indices of  $\mathbf{V}$  with higher loss
end
if  $|x| = 1$  then
     $t_{size} \leftarrow \lceil t_{size} \rceil$ 
     $\mathbf{V}^L \leftarrow \mathbf{Y} \in (\min(x) - \delta) : x_{[t_{size}]}$ 
     $\mathbf{V}^R \leftarrow \mathbf{Y} \in x_{[t_{size}]} : (\max(x) + \delta)$ 
     $l^L \leftarrow nmf(\mathbf{V}^L); l^R \leftarrow nmf(\mathbf{V}^R)$ 
    if  $l^L > l^R$  then
         $\hat{q} \leftarrow x - 1$ 
    else if  $l^R > l^L$  then
         $\hat{q} \leftarrow x$ 
end
return  $\hat{q}$ 

```

where l_i is the summed losses of \mathbf{Z}_i and l_i^* is the summed losses of \mathbf{Z}_i^* . We use Welch's t -test to determine the hypothesis. We calculate the test statistic as follows,

$$t = \frac{\bar{l}_i - \bar{l}_i^*}{\sqrt{\frac{s_i^2}{N_i} + \frac{s_i^{*2}}{N_i^*}}}.$$

If we find $\mu(l_i) < \mu(l_i^*)$, we then keep this change point, \hat{c}_i , otherwise we remove this candidate change point. This process is repeated for each candidate change point. The workflow of our FaBiSearch algorithm can be found in Algorithm 2.

2.7. Estimating stationary networks. In order to visualize the networks between each pair of change points (stationary blocks) that have been detected by FaBiSearch, we propose a new NMF based method of computing the adjacency matrix. The new method provides a sparse representation of a network while maintaining key macro level features. For each stationary block, the first step is to re-apply NMF. For each run, an adjacency matrix,

$$\mathbf{A}_{ij} = \begin{cases} 1, & \text{if } i, j \text{ are in the same cluster;} \\ 0, & \text{otherwise} \end{cases}$$

Algorithm 2: FaBiSearch algorithm for multiple change point detection. For the first iteration of the algorithm, t_{\min} and t_{\max} are time points 1 and T of \mathbf{Y} , respectively.

Inputs: \mathbf{Y} , α , δ , n_{run} , n_{reps} , r

Output: \hat{c}

if $\nexists r$ **then**

```

1  | find the optimal  $r$  for the entire input  $\{\mathbf{Y}_t\}_{t=1}^T$ .
2  For  $\{\mathbf{Y}_t\}_t^T$ : define  $t_{\min} \leftarrow t$ ;  $t_{\max} \leftarrow T$ .
3  Define  $t_{start} \leftarrow t_{\min} + \delta$ ;  $t_{end} \leftarrow t_{\max} - \delta$ .
4  Using Algorithm 1, find change point  $\hat{q}$ .
5  Define the child matrices  $\{\mathbf{Y}_t\}_{t_{\min}}^{\hat{q}}$  and  $\{\mathbf{Y}_t\}_{\hat{q}+1}^T$ 
6  For each child matrix, recursively apply steps 2 – 5 while  $t_{start} \leq t_{end}$ .
7  Define the boundaries set,  $b \leftarrow \{1, \hat{Q}, T\}$ .
   for  $i \leftarrow 2$  to  $(|b| - 2)$  do
8      $\hat{q}_i \leftarrow b(i)$ 
9      $b_i^L \leftarrow b(i - 1)$ ;  $b_i^R \leftarrow b(i + 1)$ 
10     $\mathbf{Z}_i \leftarrow \{\mathbf{Y}_t\}_{b_i^L}^{b_i^R}$  ( $\mathbf{Z}_i^L \leftarrow \{\mathbf{Y}_t\}_{b_i^L}^{\hat{q}_i}$ ;  $\mathbf{Z}_i^R \leftarrow \{\mathbf{Y}_t\}_{\hat{q}_i+1}^{b_i^R}$ )
11     $\mathbf{Z}_i^* \leftarrow \text{permute}(\mathbf{Z}_i)$ 
12
13    for  $j \leftarrow 1$  to  $n_{reps}$  do
14        $l_i(j) \leftarrow nmf(\mathbf{Z}_i^L) + nmf(\mathbf{Z}_i^R)$ 
15        $l_i^*(j) \leftarrow nmf(\mathbf{Z}_i^{*,L}) + nmf(\mathbf{Z}_i^{*,R})$ 
16    end
17    if  $\mu(l_i) < \mu(l_i^*)$  then
18        $\hat{c}_i \leftarrow \hat{q}_i$ 
19 end

```

is generated representing the cluster membership of each node (which represents each time series). By taking the average of all adjacency matrices generated over n_{run} number of runs, we obtain the corresponding consensus matrix,

$$C_{ij} = \mu(A_{ij}^1, \dots, A_{ij}^{n_{run}}), \quad 0 \leq C_{ij} \leq 1.$$

This procedure has the advantage that it can combine results across n_{run} , which may be unfavourable on their own, into an overall matrix where each entry denotes the probability of two nodes being clustered together. This is similar to stability selection in [Meinshausen and Bühlmann \(2010\)](#) and bootstrapping in [Zhu and Cribben \(2018\)](#). From here, we can apply a clustering algorithm (such as hierarchical clustering with complete-linkage) to classify cluster membership amongst nodes in the consensus matrix. This provides a clustering tree which we then cut at a predetermined number of clusters. The final product is an adjacency matrix computed as an ensemble of multiple NMF runs. The new method is shown in Figure 3. While this method provides an intuitive way to organize nodes into clusters, it requires a prespecified number of communities to be defined. In some cases or applications, this may not be known and it may not be a convenient way of interpreting interactions amongst nodes. Further, there is no way to adjust for a level of sparsity and thus many networks may be too dense to easily interpret. As such, we can also define relationships amongst nodes using the consensus matrix values and using a prespecified threshold, λ , to control the sparsity/density of the resulting adjacency matrix:

$$A_{ij} = \begin{cases} 1, & \text{if } C_{ij} > \lambda; \\ 0, & \text{otherwise.} \end{cases}$$

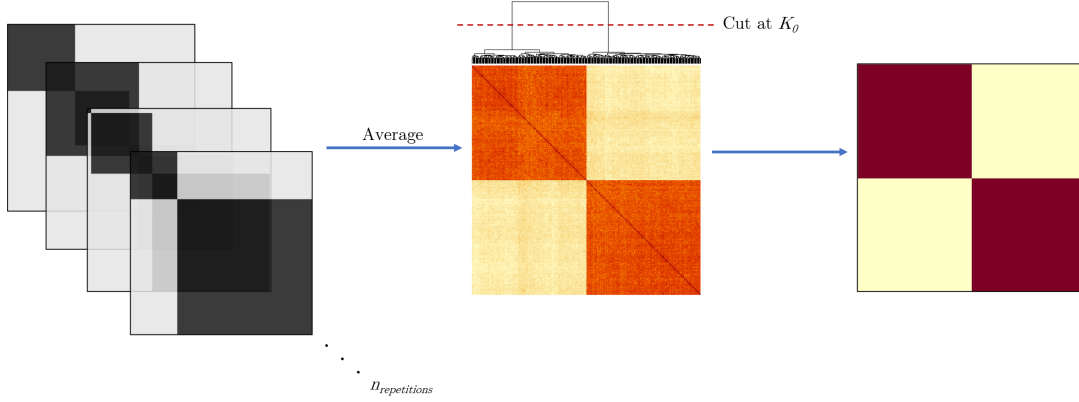


FIG 3. The workflow for visualizing networks between pairs of change points (stationary blocks). Individual adjacency matrices are calculated over n_{reps} and then averaged to find the consensus matrix. Using a clustering algorithm the consensus matrix is determined. Finally, the tree is cut at a prespecified K_0 value and the nodes are then assigned cluster membership.

3. Data.

3.1. Simulation study setup. We apply our FaBiSearch method to multiple simulation types across different dimensions. We evaluate the results by calculating the true and false positives within two margins (± 10 and ± 1 time points). As a measure of the accuracy of the detected locations in time of the detected change points compared to the location of the true change points, we also provide the scaled Hausdorff distance,

$$d_H = n_s^{-1} \max \left\{ \max_j \min_k |q_j - \hat{q}_k|, \max_k \min_j |q_j - \hat{q}_k| \right\},$$

where n_s is the length of the largest segment, \hat{q}_k are the estimated change points and q_j are the true change points. The optimal model obtains a minimum scaled Hausdorff distance.

We compare our FaBiSearch method to the Network Change Point Detection (NCPD) method (Cribben and Yu, 2017) as it is the only competing method that has software available, which is not the case for the majority of the methods mentioned in the introduction. NCPD finds change points in the network (or community) structure of multivariate high-dimensional time series data. Unlike FaBiSearch, NCPD uses binary segmentation and applies spectral clustering to find the communities based on the computed correlation matrix. The difference between the communities before and after a candidate change point are calculated using the principal angle and a stationary bootstrap is used for inference.

For each simulation, we generated 100 iterations. For FaBiSearch: we used the R package NMF (Gaujoux and Seoighe, 2010) to implement NMF, the Kullback-Leibler Divergence for the loss measure (2), a minimum distance between change points of $\delta = 50$, the number of runs $n_{\text{run}} = 100$, the number of permutations $n_{\text{reps}} = 1000$ and $\alpha = 0.001$. We did not pre-specify rank and thus let FaBiSearch find the optimal value for rank, r . For NCPD: we used a pre-specified number of clusters, K , of one greater than the actual ($K_0 + 1$), 1000 stationary bootstrap replications, a minimum distance between change points of $\delta = 50$, and $\alpha = 0.05$.

3.2. Simulated data. We now describe the simulated data. We chose simulations to emulate qualities of fMRI time series data. We progressively increased the difficulty and complexity of the simulations in order to characterize the power of FaBiSearch. All simulations are

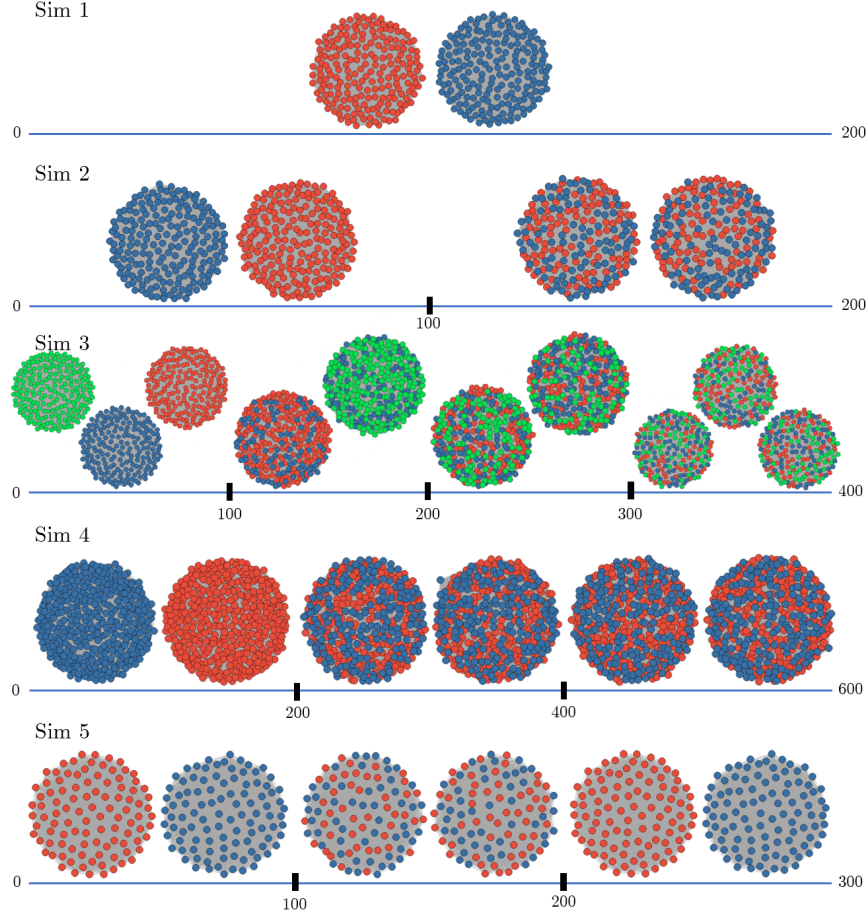


FIG 4. The true network structure of the simulations. The colors of nodes are used to show how cluster membership evolves throughout the time series. Solid black lines on the time axes indicate the location of the true change points.

multivariate high-dimensional time series with a defined clustering (or community) structure, where K_0 is the true number of clusters/communities. Data are generated from the multivariate Gaussian distribution $\mathcal{N}(0, \Sigma)$, with two structures on Σ . Structure 1 is defined as:

$$\Sigma_{ij} = \begin{cases} 0.75, & \text{if } i \neq j \text{ and } i, j \text{ are in the same cluster;} \\ 1, & \text{if } i = j; \\ 0.20, & \text{otherwise,} \end{cases}$$

and Structure 2 is defined as:

$$\Sigma_{ij} = \begin{cases} 0.75, & \text{if } i \neq j \text{ and } i, j \text{ are in the same cluster;} \\ 1, & \text{if } i = j; \\ 0.20^{|i-j|}, & \text{if } i, j \text{ are not in the same cluster.} \end{cases}$$

Simulation 1: $T = 200$, $p = 400$ time series. No change points. $K_0 = 2$. Structure 1 for Σ .

Simulation 2: $T = 200$, $p = 400$ time series. Change point at $t^* = 100$ where vertices labels are randomly reshuffled. $K_0 = 2$. Structure 1 for Σ .

Simulation 3: Structure 1 for Σ . $T = 400$, $p = 600$ time series. Change points at $t^* = 100, 200, 300$. In the first time segment, the true number of clusters $K_0 = 3$, one of which is

equally merged into the other two clusters at the first change point. Vertex labels are randomly shuffled at the second change point, while keeping $K_0 = 2$. The true number of clusters K_0 returns to 3, by moving one third of each cluster into a new, third cluster. Structure 2 for Σ .

Simulation 4: $T = 600$, $p = 800$ time series. Change points at $t^* = 200, 400$. $K_0 = 2$ throughout. At both change points, half of the vertices in each cluster are chosen at random and moved to the other cluster. Structure 2 for Σ .

Simulation 5: $T = 300$, $p = 200$ time series. Change points at $t^* = 100, 200$ time series. $K_0 = 2$. In the second time segment, the vertex labels are randomly shuffled from the first time segment. In the third time segment, the vertex labels are the same as the first time segment. Structure 2 for Σ . In this simulation, we are mimicking the ABA structure, where the subject alternates between two states.

Visualizations of these simulations are shown in Figure 4. Also, Simulations 2, 3, 4 were taken from Cribben and Yu (2017).

3.3. fMRI study setup. We also applied FaBiSearch to two fMRI data sets: a resting-state fMRI data set and a task-based fMRI data set. NMF, by definition, requires the input matrix to be non-negative however fMRI data has no such restriction. To circumvent this issue, we shift the data to make it positive by adding the same positive value to all entries of the input matrix. This ensures that the input matrix Y contains only positive values while also preserving individual variability and the covariance of ROIs. We used the same inputs for FaBiSearch for analyzing the fMRI data set as in the simulation study (Section 3.1).

3.4. Resting-state fMRI data. This data set includes 25 participants (mean age of 29.44 ± 8.64 , 10 males and 15 females) scanned at New York University over three visits (http://www.nitrc.org/projects/nyu_trt). For each visit, participants were asked to relax, remain still, and keep their eyes open. A Siemens Allegra 3.0-Tesla scanner was used to obtain the resting-state scans for each participant, however we considered only the second and third visits because they were less than an hour apart. Each visit consisted of 197 contiguous EPI functional volume scans with time repetition (TR) of 2000ms, time echo (TE) of 25ms, flip angle (FA) of 90° , 39 number of slices, matrix of 64×64 , field of view (FOV) of 192mm, and voxel size of $3 \times 3 \times 3\text{mm}^3$. Software packages AFNI (<http://afni.nimh.nih.gov/afni>) and FSL (<http://www.fmrib.ox.ac.uk>) were used for preprocessing. Motion was corrected using FSL’s `mcfliirt` (rigid body transform, cost function normalized correlation, and reference volume the middle volume). Normalization into the Montreal Neurological Institute (MNI) space was performed using FSL’s `fliirt` (affine transform, cost function, mutual information). Probabilistic segmentation was conducted to determine white matter and cerebrospinal fluid (CSF) probabilistic maps and was obtained using FSL’s `fast` with a threshold of 0.99. Nuisance signals (the six motion parameters, white matter signals, CSF signals, and global signals) were removed using AFNI’s `3dDetrend`. Volumes were spatially smoothed using a Gaussian kernel and FWHM of 6mm with FSL’s `fslmaths`. We used the work of Gordon et al. (2016) to determine the ROI atlas. The cortical surface is parcellated into 333 areas of homogenous connectivity patterns, and the time course for each is determined by averaging the voxels within each region for each subject. Regional time courses were then detrended and standardized to unit variance. Lastly, a fourth-order Butterworth filter with a 0.01-0.10 Hertz pass band was applied.

3.5. Task-based fMRI data. This data set includes 8 participants (ages 18-40) scanned at the Scientific Imaging and Brain Imaging Center at Carnegie Mellon University. Subjects in the study were asked to read Chapter 9 of *Harry Potter and the Sorcerer’s Stone* (Rowling, 2012). All subjects had previously read the book or seen the movie. The words of the story

were presented in rapid succession, where each word was presented one by one at the center of the screen for 0.5 seconds in black font on a gray background. A Siemens Verio 3.0T scanner was used to acquire the scans, utilizing a T2* sensitive echo planar imaging pulse sequence with repetition time (TR) of 2s, time echo (TE) of 29 ms, flip angle (FA) of 79°, 36 number of slices and $3 \times 3 \times 3\text{mm}^3$ voxels. Data was preprocessed as described in [Wehbe et al. \(2014\)](#). For each subject, functional data underwent realignment, slice timing correction, and co-registration with the subject’s anatomical scan, which was segmented into grey and white matter and cerebro-spinal fluid. The subject’s scans were then normalized to the MNI space and smoothed with a $6 \times 6 \times 6\text{mm}$ Gaussian kernel smoother. Data was then detrended by running a high-pass filter with a cut-off frequency of 0.005Hz after being masked by the segmented anatomical mask. Finally, the Gordon brain atlas [Gordon et al. \(2016\)](#) was again used to extract ROIs. The final time series for the task-based data contained 4 runs (324, 337, 264, and 365 time points) of 333 ROIs for each subject.

4. Results.

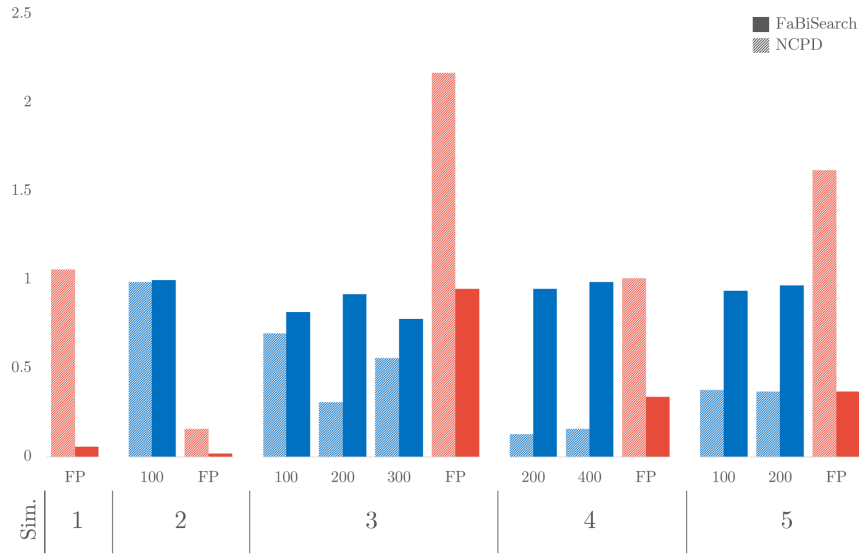


FIG 5. A plot of the true positive (blue bars) and false positive (red bars) frequency for NCPD (striped fill) and FaBiSearch (solid fill) across all the simulations using the ± 10 window.

4.1. Simulation results. In this section, we present the simulation and fMRI results. Overall, across the simulations, our FaBiSearch method outperforms NCPD ([Cribben and Yu, 2017](#)) with all the results displayed in Figure 5 (and Table 1 in the Appendix). More specifically, in Simulation 1, where there are no change points, FaBiSearch obtains a small false positive (FP) frequency of 0.04, compared to NCPD’s 1.06. In Simulation 2, the two methods perform similarly on detecting one change point. FaBiSearch finds one more true positive (TP) change point across the 100 iterations with a lower FP rate. However, once the number of time series and the complexity increases, FaBiSearch establishes a clear advantage over NCPD. For example, in Simulation 3, FaBiSearch finds 59% more TP change points than NCPD while reducing the number of FP found to 34% of those found by NCPD using the ± 10 window. The improvement of FaBiSearch over NCPD increases further in Simulation 4, where FaBiSearch finds 6.67 times more TP change points while reducing the

number of FPs to 35% of those found by NCPD using the ± 10 window. In Simulation 5, we tested the two methods on an “ABA” type structure in which the first and last clustering structures are identical. This makes the change points less discernible and thus change point detection more difficult, especially for binary segmentation methods (given the similarity between any two partitions). FaBiSearch however, performs well by detecting 95.5% of all TP change points using the ± 10 window, outperforming NCPD again. Overall, FaBiSearch finds the true change points more frequently, while drastically reducing the number of false positives found, compared to NCPD.

Across all simulations we find that the Hausdorff distance for FaBiSearch is lower than for NCPD (see Table 1 in the Appendix), indicating that the change points detected by FaBiSearch are closer to the true change points, hence, FaBiSearch outperforms NCPD. We also assessed the efficacy of NMF in estimating networks between each pair of change points (or stationary block) in the simulations. To this end, for each iteration of each simulation, we first detected the change points and hence each stationary block using FaBiSearch. Then for each stationary block, we estimated the network as described in Section 2.7 where we specified the true number of clusters, K_0 , as the cutoff point for the resulting tree. Since these adjacency matrices are symmetric, we quantified the difference between the true adjacency matrix and the NMF calculated adjacency matrix by calculating the percent overlap of the off-diagonal elements. These results are shown in Table 2 (in the Supplementary Materials). The method performs well and can recover the true network structure between change points across all simulations.

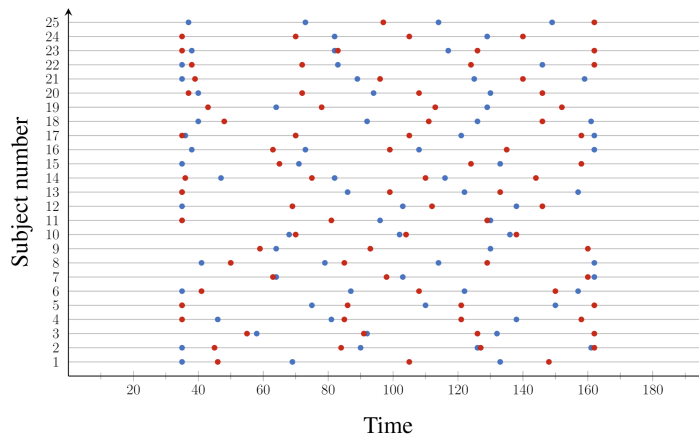


FIG 6. The detected change points for each subject in the resting-state fMRI data set. Blue and red dots denote change points for the second and third scans, respectively.

4.2. Resting-state fMRI results. Figure 6 shows the detected change points for the resting-state fMRI data set using FaBiSearch. Blue and red dots denote the change points from scans the second and third scans, respectively, which were obtained less than an hour apart (Section 3.4). We found that each subject has a unique set of change points, which is consistent with previous work (Delamillieure et al., 2010; Doucet et al., 2012), and indicates that subjects drift between different states (or functional modes) in unique ways during resting-state fMRI scanning sessions. Comparing the results across scanning sessions and between subjects, we see variability in the location and number of detected change points. Xu, Reiss and Cribben (2020) analyzed this data to study the test-retest reliability of static

FC, however, here we are considering the test-retest reliability of dynamic FC. Some subjects (e.g., subject 25) have quite different change points across the scanning sessions, while others (e.g., subjects 7, 10, and 23) have change points that are consistent across the two scans.

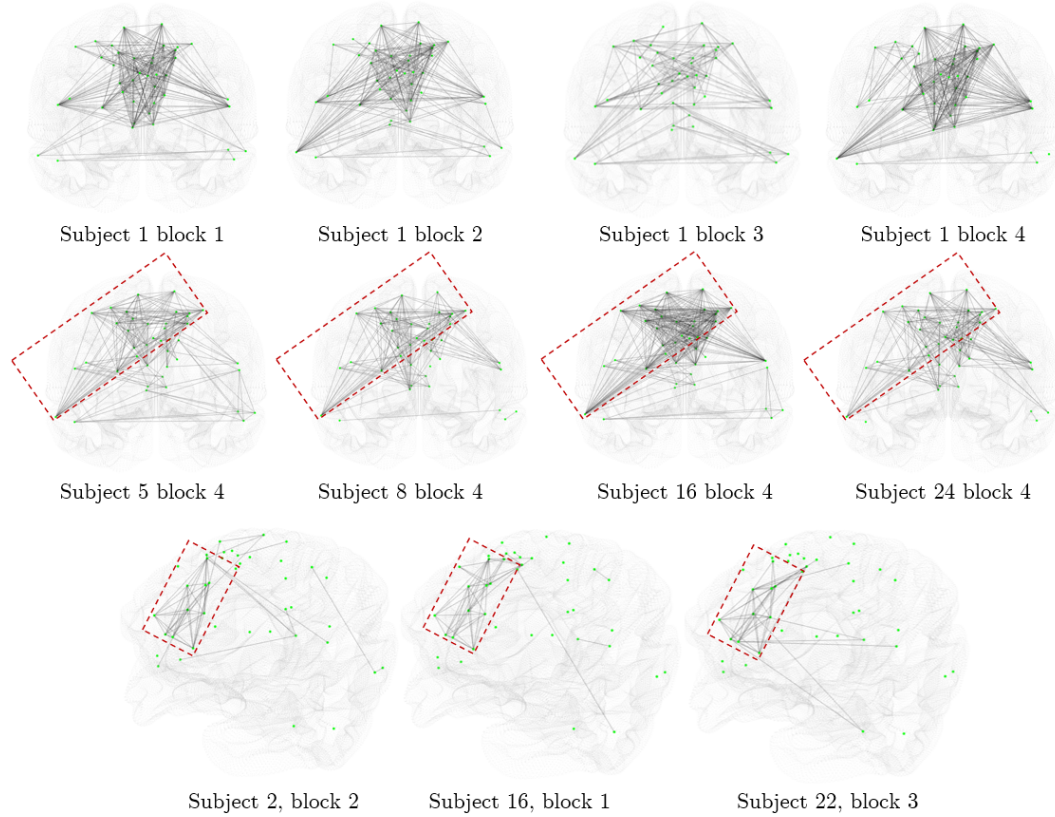


FIG 7. Networks from the resting-state fMRI data set. A comparison of the intra-subject networks in the default mode network for subject 1's second scan (top panel). A comparison of inter-subject networks of the default mode network across four different subjects in their respective final blocks of their second scan (middle panel) and across three different subjects and blocks of their second scan (bottom panel).

To further investigate the network structure, we used the NMF cluster-based graphing method described in Section 2.7. We fixed the number of runs ($n_{reps} = 100$) for calculating the consensus matrix. Previous work (Allen et al., 2012) identified 7 unique resting-state networks and so we used a prespecified cluster size, $K_0 = 7$. Figure 7 (top panel) compares the intra-subject community structure of the default mode network ($p = 41$) for subject 1's second scan. There is a clear time-varying relationship between the ROIs within this sub-network. In fact, there are substantial changes in the edge density across the segments, with segments 1 and 3 being comparatively more sparse and segments 2 and 4 being more dense. This suggests the subject's FC, and therefore mental state, was evolving during rest.

In Figure 7 (middle panel) we compare the inter-subject networks from four subjects in their respective final segments. There is a clear presence of a stable network (or sub-network) motif, which all of the subjects share. This suggests that there exists certain motifs or sub-networks in time-varying FC that remain stable across subjects. While these networks correspond to the final block of time for each subject, we do not suggest that the default mode network evolves in a similar, time-dependent manner across subjects, as during a resting-state

experiment, the subjects are unconstrained. Indeed, Figure 7 (bottom panel) shows a common network motif for subjects in different time segments. These nodes appear to connect in high degree with each other. This suggests that exists common functional states (or network features, or motifs) that are consistent across subjects in a resting-state at different time intervals. These features are meaningful given the fact that this is first study to consider over 300 fMRI time series from a change point perspective.

4.3. Task-based fMRI results. Figure 8 (left panel) shows the detected change points for the task-based fMRI data set (Section 3.5) using FaBiSearch. The results are concatenated across runs for each subject, which explains the presence of gaps, where no change points were identified. Overall, many change points were detected. In addition, there is some variance in the location and number of detected change points across subjects. Intuitively, as we consider a large number of ROIs (333) and combined with a complex and involved task such as reading, we expect FC to be constantly evolving and different for each subject based on unique factors such as age, interpretation of the story, and familiarity with the text. There are some change points however, which are consistent across subjects.

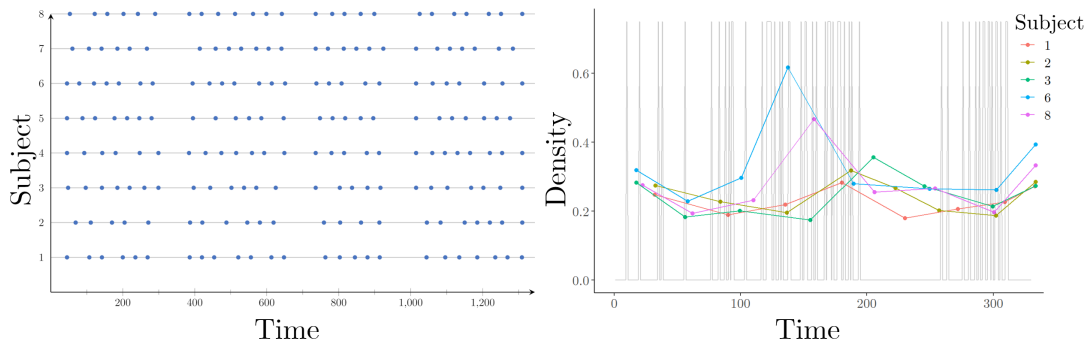


FIG 8. The detected change points for each subject in the task-based fMRI data set (left). A comparison of the density of graphs (calculated as the percent of non-zero edges in the adjacency matrix) across blocks for each subject in run 4 of the task-based fMRI study. Points are located halfway between change points. Background grey spikes correspond to the frequency of speech in Chapter 9 of Harry Potter and the Sorcerer's Stone.

Figure 9 shows the change points concatenated across subjects in a histogram. In the first run, there is a peak in the number of change points detected at bin $t = 101 : 150$ and the peak is sustained for the rest of the run. In the second run, the scanning session coincides with the following story line: after the class is left unattended by the teacher, Madam Hooch, Harry chases classmate Draco Malfoy on a broom, having never flown before. Another teacher, Professor McGonagall, spots this mischief and, instead of punishing Harry, offers him a spot as a Seeker on the Gryffindor Quidditch team. The change points detected in the $t = 551 : 600$ bin, coincide with this offer and this time point represents the beginning of Harry's Quidditch playing career, which is a recurring narrative in the book series. In the third run, Harry has accepted a wizard's duel that night with arch-rival Malfoy and is on his way with Ron to meet Malfoy at the trophy room. The change points detected peak at $t = 801 : 850$, which coincides with Hermione surprising Harry and Ron by catching them, and scolding them for trying to break school rules. In the fourth run, the three of Harry, Ron, and Hermione are almost caught by Argus Filch, the Hogwarts caretaker, and his cat, Mrs. Norris. The children scurry away but are spotted by Peeves, a poltergeist at the school. He begins shouting that the students are out of bed, which coincides with the first peak seen at times $t = 1051 : 1100$. As the children

run, they get lost and end up in a forbidden area on the third floor. The second peak seen at $t = 1201 : 1250$ coincides with the children meeting a scary and large three-headed dog.

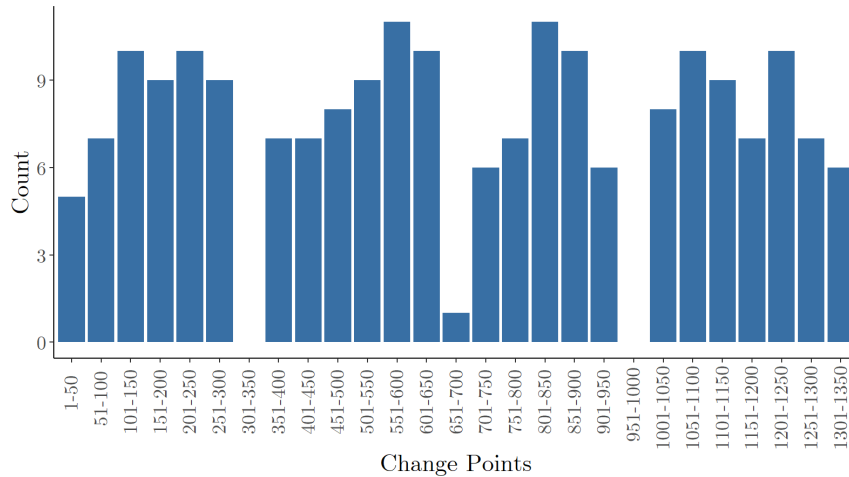


FIG 9. A histogram of change points in the task-based fMRI study across all subjects.

There are also similarities in the networks across subjects. For example, Figure 10 (top and middle panels) shows three stationary networks for three different subjects in the same run and similar time points. The networks were estimated using the NMF graphing method using a cluster cutoff value of 0.7. As expected, these networks are dense as the subjects are involved in a highly engaging task, reading. Furthermore, there is high connectivity within the visual ($p = 39$) and auditory ($p = 24$) networks, especially laterally between nodes on the left and right sides in the auditory network. Although there is some connectivity in the frontoparietal network ($p = 24$), it is not as dense as the connections between the visual and auditory regions. This supports the work of Yao, Belin and Scheepers (2011) who discovered that the auditory cortex is strongly activated during silent reading, indicative of auditory imagery – or having an “inner voice” while reading. Moreover, from the 50 strongest connections in the consensus matrix, we identified that the nodes with highest degree are in Brodmann area (BA) 22. In the left hemisphere, BA 22 contains part of Wernicke’s area (Binder, 2015) which has long been associated with language comprehension (Bogen and Bogen, 1976). Thus, it is understandable, from a network perspective, that the nodes related to this area are of high degree and have strong connections to other brain regions during reading.

We further examine commonalities in network structures across subjects in Figure 10 (bottom panel). We find that the networks of subject 7, run 2, block 1, and subject 8, run 2, block 6 are similar in many ways. Both have strong connectivity between visual nodes that are close to the brain midline. Additionally, there are many connected triples (triangles) in these nodes, with only a few connections outside of the visual community. Comparing the networks of subject 7, run 2, block 8, and subject 8, run 2, block 8, we find that these networks differ from the previously described, but are similar to each other. Both of these have densely interconnected nodes in both the visual and auditory networks, and these connections are less concentrated in the brain midline. Again, we find many triples. Subject 8, run 2, block 8 appears to have greater connectivity in the auditory communities, however both subject 7 and 8 have a few nodes on both the far left and right which are pivotal in defining these networks.

Finally, we explore the density of edges in networks and their correspondence with the story in the chapter. Figure 8 (right panel) shows the trend in edge density (calculated as the

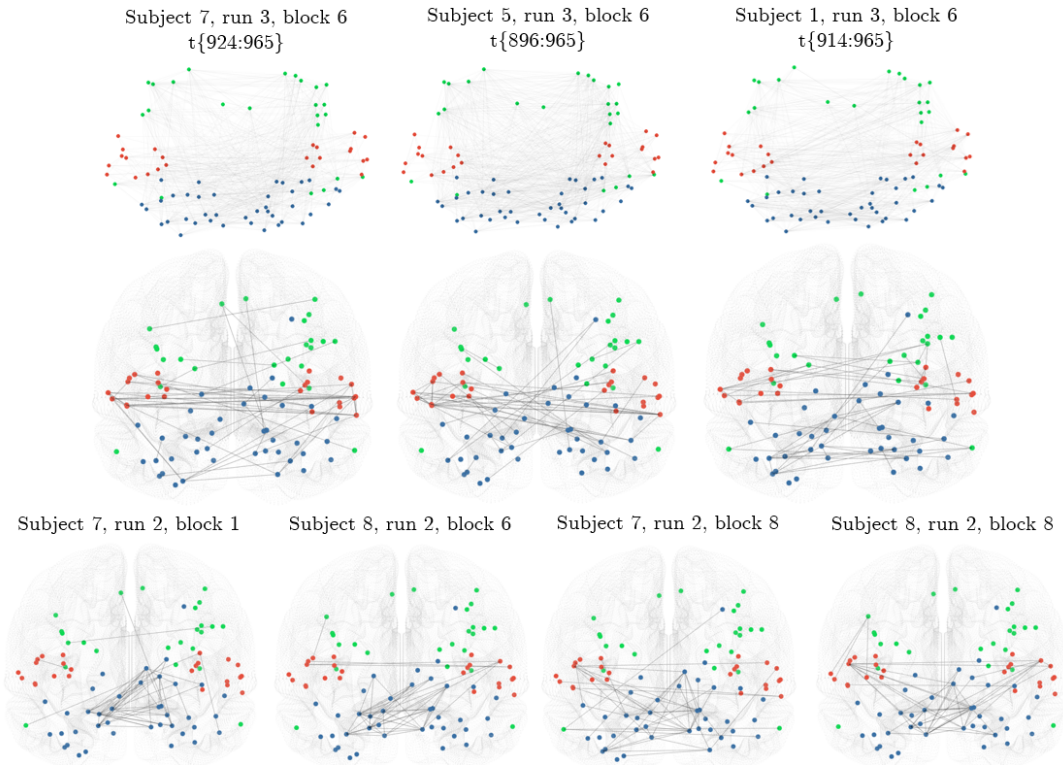


FIG 10. Networks from the task-based fMRI data set. A comparison of inter-subject networks across subjects. The top panel is a sparse version of the middle panel, where the edges represent the fifty largest inter node connection in the consensus matrix. In the bottom panel the edges represent the fifty largest inter node connection in the consensus matrix. Nodes are colored based on their community membership with blue, red and green corresponding to visual, auditory and frontoparietal networks, respectively.

percent of non-zero edges in the adjacency matrix) across blocks in the fourth run for subjects 1, 2, 3, and 8. Points are located halfway between change points. All the subjects had 8 unique blocks that initially decreased in density, increased towards the middle, decreased, and finally increased again. This suggests that there are commonalities in time-varying FC across subjects. We also compare these time series of edge densities to the frequency speech in Chapter 9 of *Harry Potter and the Sorcerer's Stone* (background grey spikes) and find that the increase in density in $t = 100 : 200$ and at $t = 300$ is related to a similar increase in characters speaking in the story. Similarly, the gaps of little ($t = 0 : 100$) and no ($t = 195 : 258$) speech correspond to lower density in the estimated networks.

5. Discussion.

5.1. *Extensions.* Non-negative matrix factorization (NMF) is an integral component of FaBiSearch and the graphical method. Our simulations and data analysis show that NMF has the capability to create a low rank approximation of the data and retain dominant network (or clustering) structures. For FaBiSearch, we concluded that the algorithms of [Lee and Seung \(2001\)](#) performed best for our data, however, we also considered other algorithms including the alternating Least Square (ALS) approach, which minimises an Euclidean-based objective function, that is regularized to favour sparse basis matrices or sparse coefficient matrices.

For more details on possible alternatives, see [Ondrus and Cribben \(2021\)](#). Furthermore, our proposed binary search method in FaBiSearch is computationally faster than standard sequential search, but is possibly limiting in that it is a purely greedy method. More exploration into non-greedy methods might yield more favourable results and/or decrease computational load. We also intend to explore other change point segmentation methods such as isolate detect [Anastasiou, Cribben and Fryzlewicz \(2020\)](#). As an extension to monitoring change points in network objects, we intend to incorporate higher order structures, such as tensors, in the NMF procedure of FaBiSearch. Finally, we have shown that the residuals between \mathbf{Y} and $\mathbf{W} \cdot \mathbf{H}$ in NMF contain important information about the clustering and dependence structure, however, its likely there are alternative methods of extracting this information.

5.2. Computation. We compared FaBiSearch to another method, Network Change Point Detection (NCPD), and found that in the same simulations FaBiSearch has a superior performance across all evaluation criteria. However, in comparison to NCPD, the computational complexity is much greater and thus the time to compute is much greater for FaBiSearch. For example, in Simulation 1, using 48 core machines with 2 Intel Platinum 8260 Cascade Lake at 2.4Ghz and 187GB of memory, FaBiSearch took 25.04 minutes on average while NCPD took 0.75 minutes on average across the 100 iterations.

6. Conclusion. In this paper, we characterize and implement a novel multiple change point detection method in the network structure between multivariate high-dimensional time series, called factorized binary search (FaBiSearch), and a method for estimating stationary network structures between detected change points. We assumed the number and location of the change points are unknown a priori. Our methods have several strengths and unique features. Firstly, FaBiSearch scales well to multivariate high-dimensional time series data. This allows us to detect change points in high-dimensional cortical atlas parcellations such as that of [Gordon et al. \(2016\)](#) to characterize whole brain dynamics. There exist very few other change point detection methods capable of handling these wide data sets and we show through simulations how FaBiSearch outperforms one of these methods.

Second, our graph estimation method finds only positive relationships between nodes. Unlike correlation measures, which can take any value in $[-1, 1]$, our new method is limited to $[0, 1]$. This is because the consensus matrix, which is the basis for this new method, is constrained to $[0, 1]$ as it is the arithmetic average of connectivity matrices which are themselves limited to $\{0, 1\}$. This makes the corresponding graph more intuitive and understandable, as anticorrelations in a FC context are difficult to interpret.

Lastly, non-negative matrix factorization (NMF) is an integral component of FaBiSearch and the graphical method. This is unique in two distinct ways. We are, to the best of our knowledge, the first to use NMF for change point detection, network estimation and to apply it specifically to fMRI data. Second, we use NMF to discover dependence structure. While some methods use clustering and/or dimension reduction techniques, these are usually applied in conjunction covariance estimation (or correlation or precision matrices). FaBiSearch solely uses NMF as a method of finding a dependence structure amongst variables, with no intermediary method of finding dependence amongst variables.

We also applied FaBiSearch to a resting-state and a task-based fMRI data set. For the resting-state experiment, we analyzed the test-retest reliability of dynamic FC, while for the task-based, we explored network dynamics during the reading of Chapter 9 in *Harry Potter and the Sorcerer's Stone*. The large scale characterizations of the FC structure has not been explored in these data sets before now. In general, we detected many change points. This suggests that regardless of the fMRI study, the FC networks are constantly evolving. We further found common states both across and within subjects in both data sets. This is encouraging as it shows the stability of some features and networks across subjects. Naturally,

FaBiSearch could also be used to determine novel biomarkers for neurological phenomena such as disease status or to find network structures corresponding to different thought processes or perceptions based on the subject specific FC.

7. Acknowledgements. This research was enabled in part by support provided by West-Grid (www.westgrid.ca) and Compute Canada (www.computeCanada.ca). The third author was supported by the Natural Sciences and Engineering Research Council (Canada) grant RGPIN-2018-06638 and the Xerox Faculty Fellowship, Alberta School of Business.

REFERENCES

- ALLEN, E. A., DAMARAJU, E., PLIS, S. M., ERHARDT, E. B., EICHELE, T. and CALHOUN, V. D. (2012). Tracking whole-brain connectivity dynamics in the resting state. *Cerebral Cortex* **bhs352**.
- ANASTASIOU, A., CRIBBEN, I. and FRYZLEWICZ, P. (2020). Cross-covariance isolate detect: a new change-point method for estimating dynamic functional connectivity. *bioRxiv*.
- AUE, A., HÖRMANN, S., HORVÁTH, L., REIMHERR, M. et al. (2009). Break detection in the covariance structure of multivariate time series models. *The Annals of Statistics* **37** 4046–4087.
- AVANESOV, V., BUZUN, N. et al. (2018). Change-point detection in high-dimensional covariance structure. *Electronic Journal of Statistics* **12** 3254–3294.
- BINDER, J. R. (2015). The Wernicke area. *Neurology* **85** 2170–2175.
- BISWAL, B., ZERRIN YETKIN, F., HAUGHTON, V. M. and HYDE, J. S. (1995). Functional connectivity in the motor cortex of resting human brain using echo-planar mri. *Magnetic Resonance in Medicine* **34** 537–541.
- BOGEN, J. E. and BOGEN, G. M. (1976). Wernicke’s region—Where is it. *Annals of the New York Academy of Sciences* **280** 834–843.
- BULLMORE, E. and SPORNS, O. (2009). Complex brain networks: graph theoretical analysis of structural and functional systems. *Nature Reviews Neuroscience* **10** 186–198.
- CHO, H. and FRYZLEWICZ, P. (2015). Multiple-change-point detection for high dimensional time series via sparsified binary segmentation. *Journal of the Royal Statistical Society: Series B (Statistical Methodology)* **77** 475–507.
- CRIBBEN, I. (2012). Detecting Dependence Change Points in Multivariate Time Series with Applications in Neuroscience and Finance, PhD thesis, Columbia University.
- CRIBBEN, I. and FIECAS, M. (2016). Functional Connectivity Analyses for fMRI Data. In *Handbook of Statistical Methods for Brain Signals and Images* (W. T. H. Ombao M. A. Lindquist and J. A. D. Aston, eds.) Chapman and Hall - CRC Press.
- CRIBBEN, I., WAGER, T. D. and LINDQUIST, M. A. (2013). Detecting functional connectivity change points for single subject fMRI data. *Frontiers in Computational Neuroscience* **7**.
- CRIBBEN, I. and YU, Y. (2017). Estimating whole-brain dynamics by using spectral clustering. *Journal of the Royal Statistical Society. Series C: Applied Statistics* **66** 607–627.
- CRIBBEN, I., HARALDSDOTTIR, R., ATLAS, L. Y., WAGER, T. D. and LINDQUIST, M. A. (2012). Dynamic Connectivity Regression: determining state-related changes in brain connectivity. *NeuroImage* **61** 907–920.
- DAI, M., ZHANG, Z. and SRIVASTAVA, A. (2019). Discovering common change-point patterns in functional connectivity across subjects. *Medical image analysis* **58** 101532.
- DEBENER, S., ULLSPERGER, M., SIEGEL, M. and ENGEL, A. K. (2006). Single-trial EEG–fMRI reveals the dynamics of cognitive function. *Trends in Cognitive Sciences* **10** 558–563.
- DELAMILLIEURE, P., DOUCET, G., MAZOYER, B., TURBELIN, M.-R., DELCROIX, N., MELLET, E., ZAGO, L., CRIVELLO, F., PETIT, L., TZOURIO-MAZOYER, N. and OTHERS (2010). The resting state questionnaire: an introspective questionnaire for evaluation of inner experience during the conscious resting state. *Brain Research Bulletin* **81** 565–573.
- DETTE, H. and WIED, D. (2016). Detecting relevant changes in time series models. *Journal of the Royal Statistical Society: Series B (Statistical Methodology)* **78** 371–394.
- DOUCET, G., NAVEAU, M., PETIT, L., ZAGO, L., CRIVELLO, F., JOBARD, G., DELCROIX, N., MELLET, E., TZOURIO-MAZOYER, N., MAZOYER, B. and OTHERS (2012). Patterns of hemodynamic low-frequency oscillations in the brain are modulated by the nature of free thought during rest. *NeuroImage* **59** 3194–3200.
- DOUGLAS, D. and PEUCKER, T. (1973). ALGORITHMS FOR THE REDUCTION OF THE NUMBER OF POINTS REQUIRED TO REPRESENT A DIGITIZED LINE OR ITS CARICATURE. *Cartographica: The International Journal for Geographic Information and Geovisualization* **10** 112–122.
- DUDA, R. O. and HART, P. E. (1974). Pattern Classification and Scene Analysis. *The Library Quarterly* **44** 258–259.

- EICHELE, T., DEBENER, S., CALHOUN, V. D., SPECHT, K., ENGEL, A. K., HUGDAHL, K., VON CRAMON, D. Y. and ULLSPERGER, M. (2008). Prediction of human errors by maladaptive changes in event-related brain networks. *Proceedings of the National Academy of Sciences* **105** 6173–6178.
- FOX, M. D., SNYDER, A. Z., VINCENT, J. L., CORBETTA, M., VAN ESSEN, D. C. and RAICHLE, M. E. (2005). The human brain is intrinsically organized into dynamic, anticorrelated functional networks. *Proceedings of the National Academy of Sciences of the United States of America* **102** 9673–9678.
- FRIGYESI, A. and HÖGLUND, M. (2008). Non-negative matrix factorization for the analysis of complex gene expression data: Identification of clinically relevant tumor subtypes. *Cancer Informatics* **6** 275–292.
- GAUJOUX, R. and SEOIGHE, C. (2010). A flexible R package for nonnegative matrix factorization. *BMC Bioinformatics* **11**.
- GIBBERD, A. J. and NELSON, J. D. B. (2014). High dimensional changepoint detection with a dynamic graphical lasso. In *2014 IEEE International Conference on Acoustics, Speech and Signal Processing (ICASSP)*. IEEE.
- GORDON, E. M., LAUMANN, T. O., ADEYEMO, B., HUCKINS, J. F., KELLEY, W. M. and PETERSEN, S. E. (2016). Generation and Evaluation of a Cortical Area Parcellation from Resting-State Correlations. *Cerebral Cortex* **26** 288–303.
- HUTCHISON, R. M., WOMELSDORF, T., ALLEN, E. A., BANDETTINI, P. A., CALHOUN, V. D., CORBETTA, M., PENNA, S. D., DUYN, J., GLOVER, G., GONZALEZ-CASTILLO, J. and OTHERS (2013). Dynamic functional connectivity: promises, issues, and interpretations. *NeuroImage* **80** 360–378.
- KAO, C., TRAPANI, L., URGAS, G. et al. (2018). Testing for instability in covariance structures. *Bernoulli* **24** 740–771.
- KIRCH, C., MUHSAL, B. and OMBAO, H. (2015). Detection of changes in multivariate time series with application to EEG data. *Journal of the American Statistical Association* **110** 1197–1216.
- KOEPCKE, L., ASHIDA, G. and KRETZBERG, J. (2016). Single and Multiple Change Point Detection in Spike Trains: Comparison of Different CUSUM Methods. *Frontiers in Systems Neuroscience* **10**.
- LEE, D. D. and SEUNG, H. S. (2001). Algorithms for Non-negative Matrix Factorization. In *Advances in Neural Information Processing Systems 13* (T. K. Leen, T. G. Dietterich and V. Tresp, eds.) 556–562. MIT Press.
- LI, T. and MA, S. (2004). IFD: Iterative feature and data clustering. *SIAM Proceedings Series* 472–476.
- LI, L., YANG, J., XU, Y., QIN, Z. and ZHANG, H. (2014). Documents clustering based on max-correntropy non-negative matrix factorization. *Proceedings - International Conference on Machine Learning and Cybernetics* **2** 850–855.
- MEINSHAUSEN, N. and BÜHLMANN, P. (2010). Stability selection. *Journal of the Royal Statistical Society: Series B (Statistical Methodology)* **72** 417–473.
- MOSQUEIRO, T., STRUBE-BLOSS, M., TUMA, R., PINTO, R., SMITH, B. H. and HUERTA, R. (2016). Non-parametric change point detection for spike trains. In *2016 Annual Conference on Information Science and Systems (CISS)* 545–550.
- OFORI-BOATENG, D., GEL, Y. R. and CRIBBEN, I. (2020). Nonparametric Anomaly Detection on Time Series of Graphs. *Journal of Computational and Graphical Statistics* **0** 1–26.
- OGAWA, S., LEE, T.-M., KAY, A. R. and TANK, D. W. (1990). Brain magnetic resonance imaging with contrast dependent on blood oxygenation. *Proceedings of the National Academy of Sciences* **87** 9868–9872.
- ONDRUS, M. and CRIBBEN, I. (2021). fabisearch: a change point detection method in the network structure of multivariate high-dimensional time series R package version 0.0.2.0000.
- PAGE, E. (1963). Controlling the standard deviation by CUSUMS and warning lines. *Technometrics* **5** 307–315.
- RAMER, U. (1972). An iterative procedure for the polygonal approximation of plane curves. *Computer Graphics and Image Processing* **1** 244–256.
- ROWLING, J. (2012). *Harry Potter and the Sorcerer's Stone*. Pottermore Limited.
- SCHRÖDER, A. L. and OMBAO, H. (2015). FreSpeD: Frequency-specific change-point detection in Epileptic Seizure Multi-Channel EEG Data.
- SPORNS, O. (2011). *Networks of the Brain*. MIT press.
- SUNDARARAJAN, R. R. and POURAHMADI, M. (2018). Nonparametric change point detection in multivariate piecewise stationary time series. *Journal of Nonparametric Statistics* 1–31.
- WEHBE, L., MURPHY, B., TALUKDAR, P., FYSHE, A., RAMDAS, A. and MITCHELL, T. (2014). Simultaneously Uncovering the Patterns of Brain Regions Involved in Different Story Reading Subprocesses. *PLOS ONE* **9** 1–19.
- XIAO, Z., HU, S., ZHANG, Q., TIAN, X., CHEN, Y., WANG, J. and CHEN, Z. (2019). Ensembles of change-point detectors: implications for real-time BMI applications. *Journal of Computational Neuroscience* **46** 107–124.
- XU, M., REISS, P. T. and CRIBBEN, I. (2020). Generalized reliability based on distances. *Biometrics*.
- YAO, B., BELIN, P. and SCHEEPERS, C. (2011). Silent reading of direct versus indirect speech activates voice-selective areas in the auditory cortex. *Journal of Cognitive Neuroscience* **23** 3146–3152.
- ZHU, Y. and CRIBBEN, I. (2018). Sparse graphical models for functional connectivity networks: best methods and the autocorrelation issue. *Brain connectivity* **8** 139–165.

Appendix

FaBiSearch							
Sim.	$\mu(r_{opt})$	t^*	TP(± 10)	FP(± 10)	TP(± 1)	FP(± 1)	Haus. dist.
1	3.08	N/A	N/A	0.04	N/A	0.04	N/A
2	4.66	100	1.00	0.02	0.86	0.16	0.0082
3	5.50	100	0.80	0.74	0.44	1.70	0.0623
		200	0.92		0.66		
		300	0.78		0.44		
4	6.84	200	0.95	0.35	0.82	0.62	0.1125
		400	0.99		0.85		
5	5.49	100	0.94	0.29	0.77	0.68	0.0345
		200	0.97		0.75		

NCPD							
Sim.	K	t^*	TP(± 10)	FP(± 10)	TP(± 1)	FP(± 1)	Haus. dist.
1	3	N/A	N/A	1.06	N/A	1.06	N/A
2	3	100	0.99	0.16	0.81	0.34	0.0390
3	4	100	0.70	2.17	0.42	3	0.1000
		200	0.31		0.06		
		300	0.56		0.26		
4	3	200	0.13	1.01	0.02	1.23	0.5283
		400	0.16		0.05		
5	3	100	0.38	1.62	0.15	2.13	0.1131
		200	0.37		0.09		

TABLE 1

The simulation results for FaBiSearch (top) and NCPD (bottom). Sim., $\mu(r_{opt})$, t^* , $TP(\pm i)$, $FP(\pm i)$, and Haus. dist. denote the simulation number, average optimal rank, true change point(s), true positive within i time points, false positives outside i time points, and Hausdorff distance within 10 time points, respectively. K in the NCPD table denotes the number of clusters used for the spectral clustering algorithm.

Simulation	1	2	3	4	5
% correct	100	100	98.76	99.69	99.50

TABLE 2

For each simulation, a comparison of the true networks and the estimated networks using NMF between each pair of change points (stationary blocks). The percentage was calculated as the proportion of overlap in the off-diagonal elements between the true adjacency matrix and the estimated NMF adjacency matrix.